Bioorganic Chemistry 87 (2019) 409–416

Contents lists available at ScienceDirect

Bioorganic Chemistry

journal homepage: www.elsevier.com/locate/bioorg

Hyperpatulols A–I, spirocyclic acylphloroglucinol derivatives with anti-migration activities from the flowers of *Hypericum patulum*

Yang-Yang Liu, Zhen Ao, Qi-Qi Xu, Dong-Rong Zhu, Chen Chen, Xiao-Bing Wang, Jian-Guang Luo*, Ling-Yi Kong*

Jiangsu Key Laboratory of Bioactive Natural Product Research and State Key Laboratory of Natural Medicines, School of Traditional Chinese Pharmacy, China Pharmaceutical University, 24 Tong Jia Xiang, Nanjing 210009, People's Republic of China

ARTICLE INFO

Keywords:
Hypericum patulum
Spirocyclic acylphloroglucinol derivatives
ECD exciton chirality method
ECD calculation
Anti-migration activity

ABSTRACT

Nine new spirocyclic acylphloroglucinol derivatives, hyperpatulols A–I (**1**–**9**), were characterized from the flowers of *Hypericum patulum*. Their structures were elucidated by the basic analysis of the obtained spectroscopic data, and their absolute configurations were assigned by both the electronic circular dichroism (ECD) exciton chirality method and ECD calculation. The evaluation of their anti-migration effects on U2-OS human osteosarcoma cells showed that compound **4** exhibited moderate inhibitory activity in a dose-dependent manner. Further pharmacological studies revealed that **4** could regulate the expression of the proteins Vimentin and E-cadherin.

1. Introduction

Hypericum, an important genus in the family Guttiferae, has been reported to contain multiple metabolites, including naphthodianthrones [1], xanthones [2], flavonoids [3], and prenylated acylphloroglucinols [4,5]. Among them, polyprenylated acylphloroglucinols feature a highly oxygenated bicyclo-[3.2.1]-octane-2,4,8-trione or bicyclo-[3.3.1]-nonane-2,4,9-trione core decorated with prenyl or geranyl side chains and show considerable structural diversity [6]. Further pharmacological investigations revealed that these kinds of metabolites exhibited broad biological activities, including antitumor [7,8], antibacterial [9], antioxidant [10], anti-HIV [11], antiangiogenic [12] and anti-inflammatory activities [13]. Due to their structural complexity and diversity and potential pharmacological effects, these kinds of metabolites have attracted broad scientific interest [14,15].

H. patulum Thunb. ex Murray has been used in China to treat a variety of diseases, including bacterial diseases, hepatitis, and nasal hemorrhage [16]. Given that two novel cage-like prenylated acylphloroglucinols have been reported from this medicinal plant [17], the phytochemical constituents of its flowers were investigated to obtain an unprecedented homoadamantane-type acylphloroglucinol [18]. During our continuing to search for the PPAPs with novel structures and significant pharmacological activities, nine new spirocyclic acylphloroglucinol derivatives, hyperpatulols A–I (**1**–**9**), were obtained. Herein, the isolation procedure and structural elucidation of compounds **1**–**9** along with their anti-migration activities are discussed.

2. Materials and methods

2.1. General experimental procedures

A JASCOP-1020 polarimeter (Jasco, Japan) was used to record the optical rotation values. A Bruker Tensor 27 spectrometer (Bruker, Germany) gave the IR spectra. UV spectra were obtained on a UV-2450 UV/vis spectrophotometer (Shimadzu, Japan). HRESIMS spectra were performed on an Agilent 6520B Q-TOF instrument (Agilent Technologies, USA). A JASCO-810 spectrometer (Jasco, Japan) was used to measure the ECD spectra. NMR spectra were acquired on a Bruker AVIII-600 NMR instrument equipped with CryoProbe (Bruker, Germany). Preparative HPLC (*Prep*-HPLC) was carried out on a Shimadzu LC-20AR (Shimadzu, Japan) equipped with a Shimadzu ODS column (250 mm × 20 mm, 10 μm). The detection wavelengths were 210 and 270 nm.

2.2. Plant material

Air-dried flowers of *H. patulum* employed in this work were collected from Yunnan Province, People's Republic of China, in August

* Corresponding author.
E-mail addresses: luojg@cpu.edu.cn (J.-G. Luo), cpu_lykong@126.com (L.-Y. Kong).

https://doi.org/10.1016/j.bioorg.2019.03.025
Received 10 February 2019; Received in revised form 6 March 2019; Accepted 13 March 2019
Available online 20 March 2019
0045-2068/

2017, and the identification of the sample was carried out by *Prof.* Mian Zhang. A sample specimen (2017-HPF) was stored in the Department of Natural Medicinal Chemistry, China Pharmaceutical University.

2.3. Extraction and isolation

The dried powder of flowers of *H. patulum* (5.0 kg) was extracted under ultrasonic agitation with 95% ethanol. The extract (1.17 kg) was dispersed with H_2O and extracted with petroleum ether (PE). The PE extract (191 g) was loaded onto a silica gel column with petroleum ether-ethyl acetate (1:0–8:2) as the eluent to afford five major fractions A–E. B (34.1 g) was then separated on an RP-C_{18} column (MeCN-H_2O, 60–90%) to give subfractions B1–B5. B2 (12.0 g) was fractioned by the RP-C_{18} column (MeOH-H_2O, 70–90%) to obtain fractions B2A–B2E. B2A (1.85 g) was chromatographed on an RP-C_{18} column (MeCN-H_2O, 60–90%) to yield four major subfractions, B2A1–B2A4. B2A2 (67.1 mg) was subsequently purified by *Prep*-HPLC (MeOH − H_2O, 75%) to afford compounds **9** (7.5 mg, t_R 20.6 min). Compounds **7** (5.5 mg, t_R 22.8 min) and **8** (5.6 mg, t_R 24.5 min) were yielded from B2A3 (555.8 mg), and compound **1** (14.5 mg, t_R 28.6 min) was isolated from B2A4 (576.0 mg) using the same procedure. Fraction B2C (6.19 g) was subjected to an RP-C_{18} column (MeOH–H_2O, 70–90%) to give eight subfractions, B2C1–B2C8. The *Prep*-HPLC purification of B2C1 (273.5 mg) yielded compound **3** (1.7 mg, t_R 18.6 min). Compounds **4** (27.4 mg, t_R 22.8 min) and **6** (42.5 mg, t_R 25.6 min) were obtained from B2C2 (184.9 mg) and B2C3 (438.7 mg) using the same procedure, respectively. Compound **2** (15.6 mg, t_R 30.4 min) was obtained from B2C6 (606.7 mg), and **5** (265.6 mg, t_R 35.8 min) was separated from B2C7 (627.7 mg) using the *Prep*-HPLC (MeOH–H_2O, 85%).

2.4. Spectroscopic data

Hyperpatulol A ***(1)***: light yellow gum; $[\alpha]_D^{25}$ + 34.2 (*c* 0.1, MeOH); UV (MeOH) λ_{max} (log ε) 203 (2.14), 246 (1.12), 281 (1.17) nm; ECD (MeOH) λ ($\Delta\varepsilon$) 240 (−7.55), 274 (−1.51), 288 (−1.98), 310 (+7.13) nm; IR (KBr) ν_{max} 3344, 2964, 2927, 1570, 1508, 1451, 1378 cm^{-1}; ^1H and ^{13}C NMR data, see Table 1; HRESIMS *m/z* 557.2869 $[M+Na]^+$ (calcd for $C_{33}H_{42}O_6Na$, 557.2874).

Hyperpatulol B ***(2)***: light yellow gum; $[\alpha]_D^{25}$ − 35.2 (*c* 0.1, MeOH); UV (MeOH) λ_{max} (log ε) 202 (3.19), 262 (2.02) nm; ECD (MeOH) λ ($\Delta\varepsilon$) 201 (+6.29), 233 (−4.32), 260 (+2.68), 290 (−7.27) nm; IR (KBr) ν_{max} 2970, 2933, 1699, 1605, 1452, 1384 cm^{-1}; ^1H and ^{13}C NMR data, see Table 1; HRESIMS *m/z* 573.2825 $[M+Na]^+$ (calcd for $C_{33}H_{42}O_7Na$, 573.2823).

Hyperpatulol C ***(3)***: light yellow gum; $[\alpha]_D^{25}$ + 18.8 (*c* 0.1, MeOH); UV (MeOH) λ_{max} (log ε) 203 (1.98), 243 (1.52), 282 (2.95) nm; ECD (MeOH) λ ($\Delta\varepsilon$) 221 (+3.86), 268 (+5.20), 297 (−5.71), 326 (+4.53) nm; IR (KBr) ν_{max} 3423, 2961, 2922, 2838, 1670, 1459, 1377 cm^{-1}; ^1H and ^{13}C NMR data, see Table 1; HRESIMS *m/z* 469.2560 $[M+Na]^+$ (calcd for $C_{26}H_{38}O_6Na$, 469.2561).

Hyperpatulol D ***(4)***: light yellow gum; $[\alpha]_D^{25}$ + 2.2 (*c* 0.1, MeOH); UV (MeOH) λ_{max} (log ε) 203 (2.01), 282 (2.45) nm; ECD (MeOH) λ ($\Delta\varepsilon$) 215 (+11.26), 243 (+6.24), 277 (+3.10), 319 (−5.67) nm; IR (KBr) ν_{max} 3379, 2966, 2930, 2874, 1717, 1682, 1640, 1577, 1456, 1383 cm^{-1}; ^1H and ^{13}C NMR data, see Table 2; HRESIMS *m/z* 469.2562 $[M+Na]^+$ (calcd for $C_{26}H_{38}O_6Na$, 469.2561).

Hyperpatulol E ***(5)***: light yellow gum; $[\alpha]_D^{25}$ + 10.6 (*c* 0.1, MeOH); UV (MeOH) λ_{max} (log ε) 203 (1.97), 282 (2.64) nm; ECD (MeOH) λ ($\Delta\varepsilon$) 217 (+15.36), 241 (+10.25), 274 (+7.98), 319 (−7.08) nm; IR (KBr) ν_{max} 3366, 2966, 2932, 1717, 1681, 1572, 1457, 1381 cm^{-1}; ^1H and ^{13}C NMR data, see Table 2; HRESIMS *m/z* 483.2715 $[M+Na]^+$ (calcd for $C_{27}H_{40}O_6Na$, 483.2717).

Hyperpatulol F ***(6)***: light yellow gum; $[\alpha]_D^{25}$ + 14.0 (*c* 0.1, MeOH); UV (MeOH) λ_{max} (log ε) 280 (2.25) nm; ECD (MeOH) λ ($\Delta\varepsilon$) 239 (+3.35), 250 (+1.55), 269 (+6.03), 292 (−0.73), 304(+2.87) nm; IR (KBr) ν_{max} 3367, 2969, 2932, 2874, 1669, 1587, 1459, 1384 cm^{-1}; ^1H and ^{13}C NMR data, see Table 2; HRESIMS *m/z* 485.2511 $[M+Na]^+$ (calcd for $C_{26}H_{38}O_7Na$, 485.2510).

Hyperpatulol G ***(7)***: light yellow gum; $[\alpha]_D^{25}$ − 40.6 (*c* 0.1, MeOH); UV (MeOH) λ_{max} (log ε) 265 (1.74) nm; ECD (MeOH) λ ($\Delta\varepsilon$) 213 (+4.87), 241 (−8.51), 268 (−2.56), 290 (−18.49), 334(+2.82) nm; IR (KBr) ν_{max} 3496, 2966, 2931, 2874, 1696, 1625, 1457, 1378 cm^{-1}; ^1H and ^{13}C NMR data, see Table 3; HRESIMS *m/z* 465.2614 $[M+Na]^+$ (calcd for $C_{27}H_{38}O_5Na$, 465.2611).

Hyperpatulol H ***(8)***: light yellow gum; $[\alpha]_D^{25}$ − 31.2 (*c* 0.1, MeOH); UV (MeOH) λ_{max} (log ε) 264 (3.43) nm; ECD (MeOH) λ ($\Delta\varepsilon$) 210 (+4.52), 244 (−2.78), 265 (+0.35), 283 (−8.85), 335(+0.93) nm; IR (KBr) ν_{max} 2965, 2930, 2875, 1697, 1622, 1457, 1377 cm^{-1}; ^1H and ^{13}C NMR data, see Table 3; HRESIMS *m/z* 465.2608 $[M+Na]^+$ (calcd for $C_{27}H_{38}O_5Na$, 465.2611).

Hyperpatulol I ***(9)***: light yellow gum; $[\alpha]_D^{25}$ − 9.4 (*c* 0.1, MeOH); UV (MeOH) λ_{max} (log ε) 203 (1.76), 235 (0.96), 275 (0.74) nm; ECD (MeOH) λ ($\Delta\varepsilon$) 233 (+1.45), 276 (−1.57), 298 (+0.30), 327 (−0.70) nm; IR (KBr) ν_{max} 3433, 2970, 1713, 1451, 1384 cm^{-1}; ^1H and ^{13}C NMR data, see Table 3; HRESIMS *m/z* 451.2452 $[M+Na]^+$ (calcd for $C_{26}H_{36}O_5Na$, 451.2455).

Table 1
^1H (600 MHz) and ^{13}C (150 MHz) NMR Data of Compounds **1–3** in $CDCl_3$.

	Hyperpatulol A (**1**)		Hyperpatulol B (**2**)		Hyperpatulol C (**3**)	
Position	δ_C	δ_H, mult (*J*, Hz)	δ_C	δ_H, mult (*J*, Hz)	δ_C	δ_H, mult (*J*, Hz)
1	193.3		194.2		198.7	
2	112.8		113.3		110.6	
3	193.3		195.2		196.1	
4	62.5		62.0		64.4	
5	213.9		208.0		208.2	
6	61.4		61.0		56.3	
7	40.8	a, 1.82, m b, 1.72, m	27.0	a, 1.81, m b, 1.69, m	32.3	1.81, m
8	43.8	1.33, m	46.6	1.94, m	47.9	1.29, m
9	79.9		78.4		78.9	
10	40.8	a, 1.84, m b, 1.70, m	40.5	1.81, m	41.0	a, 2.14, brd (15.0) b, 1.91, brd (15.0)
11	20.9	1.74, m	22.7	a, 1.81, m b, 1.47, m	22.8	1.44, m
12	51.1	1.73, m	47.1	1.69, m	51.6	1.81, m
13	68.8		85.4		72.5	
14	37.8	a, 2.35, m b, 1.43, m	36.2	2.10, m	42.0	a, 2.14, d (14.8) b, 1.93, d (14.8)
15	29.1	1.22, s	19.1	1.24, s	23.9	1.24, s
16	26.8	1.26, s	26.6	1.28, s	26.6	1.23, s
17	34.9	2.83, m	37.6	2.62, m	21.7	1.44, s
18	118.1	4.92, m	117.8	4.83, t (8.1)	38.9	a, 2.69, m b, 2.42, m
19	136.8		137.4		117.3	4.74, t (8.0)
20	18.3	1.66, s	18.0	1.57, s	137.3	
21	26.3	1.64, s	26.1	1.59, s	17.8	1.47, s
22	41.9	a, 2.68, m b, 2.56, m	37.9	2.77, m	25.9	1.57, s
23	116.6	4, 76, m	117.7	4.95, t (7.5)	207.3	
24	139.4		137.5		35.0	3.63, m
25	18.0	1.49, s	18.0	1.57, s	18.7	1.15, d (6.7)
26	26.1	1.54, s	26.0	1.62, s	19.7	1.21, d (6.7)
27	197.9		196.5			
28	137.4		136.6			
29	127.8	7.50, m	127.9	7.55, m		
30	128.2	7.42, m	128.1	7.43, m		
31	132.3	7.53, m	132.3	7.55, m		
32	128.2	7.42, m	128.1	7.43, m		
33	127.8	7.50, m	127.9	7.55, m		

Table 2
^{1}H (600 MHz) and ^{13}C (150 MHz) NMR Data of Compounds **4–6** in $CDCl_3$.

	Hyperpatulol D (**4**)		Hyperpatulol E (**5**)		Hyperpatulol F (**6**)	
Position	δ_C	δ_H, mult (*J*, Hz)	δ_C	δ_H, mult (*J*, Hz)	δ_C	δ_H, mult (*J*, Hz)
1	198.3		198.4		198.1	
2	110.9		111.6		110.1	
3	199.2		199.4		195.7	
4	64.7		64.6		60.3	
5	208.3		208.4		214.1	
6	56.7		56.7		55.9	
7	29.8	a, 1.91, dd (13.1, 4.5) b, 1, 65, brd (13.1)	30.6	a, 1.91, brd (14.4) b, 1.65, brd (14.4)	30.8	a, 2.02, brd (12.1) b, 1.66, brd (12.1)
8	44.7	1.70, m	44.5	1.47, m	54.8	1.70, m
9	79.5		79.6		80.4	
10	40.0	1.79, m	40.2	1.73, m	39.1	a, 1.83, m b, 1.70, m
11	21.0	1.72, m	21.0	a, 1.73, m b, 1.46, m	31.4	a, 2.14, m b, 1.70, m
12	50.8	2.11, dd (14.4, 2.0)	50.9	1.72, m	81.5	
13	70.6		70.3		74.1	
14	44.6	a, 1.85, d (14.4) b, 1.53, d (14.4)	44.1	a, 2.08, dd (14.5, 1.9) b, 1.94, brd (14.5)	33.8	a, 2.33, d (15.2) b, 2.06, d (15.2)
15	29.1	1.20, s	29.2	1.21, s	24.2	1, 37, s
16	26.5	1.28, s	26.5	1.27, s	24.2	1.16, s
17	24.6	1.40, s	25.0	1.40, s	21.4	1.57, s
18	37.5	a, 2.70, dd (13.7, 8.2) b, 2.53, dd (13.7, 8.2)	37.2	a, 2.73, dd (13.8, 7.9) b, 2.56, dd (13.8, 7.9)	41.9	a, 2.61, dd (13.5, 8.7) b, 2.50, dd (13.5, 8.7)
19	118.2	4.77, t (8.2)	118.4	4.79, t (7.9)	116.6	4.67, t (8.7)
20	136.8		136.6		138.9	
21	17.9	1.51, s	18.0	1.54, s	17.9	1.42, s
22	26.0	1.59, s	26.1	1.59, s	26.0	1.57, s
23	207.5		207.6		209.6	
24	34.8	3.54, m	41.3	3.44, m	36.3	3.78, m
25	18.6	1.17, d (2.7)	27.7	a, 1.75, m b, 1.46, m	18.3	1.18, d (6.9)
26	20.3	1.18, d (2.7)	11.9	0.89, t (7.4)	20.2	1.26, d (6.9)
27			16.8	1.17, d (6.7)		

Table 3
^{1}H (600 MHz) and ^{13}C (150 MHz) NMR Data of Compounds **7–9** in $CDCl_3$.

	Hyperpatulol G (**7**)		Hyperpatulol H (**8**)		Hyperpatulol I (**9**)	
Position	δ_C	δ_H, mult (*J*, Hz)	δ_C	δ_H, mult (*J*, Hz)	δ_C	δ_H, mult (*J*, Hz)
1	197.7		197.9		198.1	
2	111.9		112.1		111.8	
3	177.7		177.3		177.3	
4	59.1		58.9		58.9	
5	208.3		208.7		208.7	
6	59.5		59.6		59.7	
7	32.5	a, 1.91, m b, 1.54, m	34.0	a, 2.02, dd (13.5, 4.6) b, 1.52, m	34.0	a, 2.04, m b, 1.53, dd (10.0, 3.4)
8	49.0	1.21, dd (4.3, 12.3)	44.4	1.91, m	44.4	1.93, m
9	76.6		79.5		79.6	
10	40.0	a, 1.89, m b, 1.72, m	37.6	a, 1.91, m b, 1.78, m	37.6	a, 2.21, m b, 1.69, m
11	22.4	a, 1.72, m b, 1.37, m	23.9		23.9	1.79, m
12	47.6	2.04, td (12.0, 6.0)	44.8	2.40, m	44.8	1.93, m
13	92.0		94.7		94.8	
14	44.7	a, 2.14, d (11.9) b, 1.97, d (11.9)	38.2	a, 2.19, d (12.2) b, 1.78, m	38.2	a, 2.21, d (16.2) b, 1.81, m
15	21.6	1.52, s	23.5	1.48, s	23.6	1.50, s
16	26.4	1.25, s	28.7	1.28, s	28.8	1.30, s
17	26.1	1.32, s	25.8	1.29, s	26.0	1.32, s
18	34.9	2.61, brd (7.8)	35.0	2.59, m	35.0	2.61, d (7.4)
19	119.9	4.98, t (7.8)	119.6	4.98, t (7.7)	119.7	4.99, t (7.4)
20	135.1		135.5		135.6	
21	17.8	1.62, s	18.0	1.56, s	18.0	1.58, s
22	25.9	1.57, s	25.9	1.60, s	26.0	1.32, s
23	203.7		203.6		203.7	
24	46.7	3.01, m	46.6	3.07, m	39.9	3.22, m
25	25.5	a, 1.72, m b, 1.34, m	25.6	a, 1.78, m b, 1.36, m	18.1	1.13, d (7.0)
26	11.6	0.86, t (7.6)	11.8	0.90, t (7.4)	18.5	1.07. d (7.0)
27	15.4	1.10, d (6.9)	15.8	1.03, d (7.0)		

2.5. Anti-migration activity

2.5.1. Cell lines and cell culture

The human osteosarcoma cell lines U2-OS was purchased from the Cell Bank of Biochemistry and Cell Biology, Chinese Academy of Sciences (Shanghai, China). U2-OS cells were cultured in an RPMI-1640 medium containing 10% fetal bovine serum in a humidified environment without *mycoplasma* at 37 °C and 5% CO_2.

2.5.2. Cytotoxicity assay

MTT method was used to evaluate the cytotoxicity of the new isolates against U2-OS cell lines. Cells were cultured in the 96-well microplates for 24 h in a cell incubator. Subsequently, cells were cultured for additional 24 h in the culture medium containing various concentrations of compounds, followed by addition of 20 ml MTT (5 mg/ml) into each well and incubation for 4 h. Then, the culture medium was aspirated off, and DMSO (150 ml) was added by constant shaking for 10 min. A Spectramax Plus 384 Universal Microplate Reader was used to detect the optical density with 570 nm as the detect wavelength. And the reference wavelength was 630 nm. The cell viability was calculated and presented as IC_{50} values.

2.5.3. Wound healing assay

Cells (2×10^5 cells/ml) were cultured for 24 h in the 6-well plate, followed by incubation for another 12 h in the serum-free medium. Then, the confluent cells were scraped to create a mechanical wound in the middle of each well and incubated by different compounds with various concentrations. Cells were imaged by a phase-contrast microscope after scrapping at 0 and 24 h.

2.5.4. Transwell assay

A Transwell chamber (Corning, USA) with 8 μm pore size was used to determine the cell migration. The upper chamber was added the serum-free medium with 6×10^4 cells, whereas the lower chamber was the 10% FBS medium. After incubation for 24 h, cells in the upper chamber were removed and fixed with paraformaldehyde in the lower surface of the chamber membrane. Crystal violet was used to stain. A phase-contrast microscopy was used to count migrated cells.

2.5.5. Western blot analysis

After treated with compounds by various concentrations, cells were rinsed twice by PBS, followed by lysing in the RIPA buffer. After separation on SDS polyacrylamide gels, the cell lysates were transferred to PVDF membranes (Bio-Rad, Hercules, CA) to block nonspecific binding of the membranes to TBS-T (0.1% Tween) containing 5% nonfat milk for 1 h. The primary antibodies were used to immunoblot the membranes overnight at 4 °C, followed by incubating the membranes with HRP-conjugated goat anti-rabbit secondary antibody for 2 h. A ChemiDOC™ system (Bio-Rad, Hercules, CA) was used to detect the protein bands. The primary antibodies and HRP-conjugated goat anti-

rabbit secondary antibody were obtained from Cell Signaling Technology.

3. Results and discussion

3.1. Structure elucidation

Hyperpatulol A (**1**) was obtained as a light yellow gum. Its molecular formula of $C_{33}H_{42}O_6$ was assigned by the observed sodium adduct ion peak at *m/z* 557.2869 $[M+Na]^+$ and its ^{13}C NMR data, corresponding to 13 indices of hydrogen deficiency. Its IR data exhibited the characteristic absorption bands of hydroxyl (3344 cm^{-1}), carbonyl (1675 cm^{-1}) and aromatic ring (1570, 1508 and 1451 cm^{-1}). Its ^1H NMR data (Table 1) showed the signals for one monosubstituted phenyl group at δ_H 7.53 (1H, m), 7.50 (2H, m), and 7.42 (2H, m), two olefinic protons at δ_H 4.92 (1H, m), and 4.76 (1H, m), and six methyl singlets at δ_H 1.66, 1.64, 1.54, 1.49, 1.26, and 1.22. Its ^{13}C NMR data (Table 1) combined with the HSQC and HMBC spectra displayed 33 signals, which were assigned to an unconjugated carbonyl group (δ_C 213.9), an enolized 1,3-diketo functionality (δ_C 193.3, 112.8, and 193.3), one benzoyl group (δ_C 197.9, 137.4, 132.3, 128.2 × 2, 127.8 × 2), two prenyl groups (δ_C 34.9, 118.1, 136.8, 18.3, 26.3; 41.9, 116.6, 139.4, 18.0, 26.1), two oxygenated tertiary carbons (δ_C 79.9 and 68.8), two sp^3 quaternary carbons (δ_C 62.5 and 61.4), two sp^3 methines (δ_C 43.8 and 51.1), four sp^3 methylenes (δ_C 40.8 × 2, 37.8 and 20.9), and two tertiary methyls (δ_C 29.1 and 26.8). These data revealed that **1** was an analogue of hyperbeanol C [19]. A comparison of their ^{13}C NMR data disclosed the differences in signals of C-1 and C-3 between **1** and hyperbeanol C. The shielded chemical shifts of C-1 (δ_C 193.3 in **1**; δ_C 196.9 in hyperbeanol C) and C-3 (δ_C 193.3 in **1**; δ_C 195.6 in hyperbeanol C) suggested that the enol group at C-1 and the carbonyl group at C-3 in hyperbeanol C were exchanged in **1** [11,20–22] (Fig. 2). This deduction was further confirmed by the correlations from H-7a (δ_H 1.82) and H-14a (δ_H 2.35) to C-3 (δ_C 193.3), C-4 (δ_C 62.5), and C-5 (δ_C 213.9), and from H_2-17 (δ_H 2.83) and H-22a (δ_H 2.68) to C-1 (δ_C 193.3), C-5 (δ_C 213.9), and C-6 (δ_C 61.4) in its HMBC spectrum.

The relative configuration of compound **1** was determined by the ROESY experiment recorded in $CDCl_3$ (Fig. 2). The ROE interactions of H-12 with H-7b and H-14b indicated that H-7b, H-12, and H-14b were co-facial with the axial orientation, suggesting the chair conformation of the cyclohexane moiety. Subsequently, the obvious ROE correlations of H-8/H-14a, Me-15/H-14a, and H-8/Me-15 revealed that H-8 and H-14a were β-oriented, indicating the trans-fused conformation of the cyclohexane and cyclopentane moieties. The β-orientation for Me-15 and Me-16 was confirmed by the observed ROE correlations of H-8/Me-16, H-8/Me-15, H-14a/Me-16, and H-14a/Me-15. In addition, the ROE interactions of H-29 with H-14a and Me-15 revealed that the benzoyl group was at the upper side of the cyclohexane moiety. Therefore, the structure of **1** was defined.

The molecular formula of hyperpatulol B (**2**), $C_{33}H_{42}O_7$, was confirmed by analysis of its ^{13}C NMR and HRESIMS spectra (*m/z* 573.2825 $[M+Na]^+$), with one more oxygen atom than that of **1**. The ^1H and ^{13}C NMR data, assigned by HSQC and HMBC experiments, showed that compound **2** had identical numbers of methyl, methine, methylene, and quaternary carbon to **1**, suggesting that **2** should be a hydroperoxyl derivative of **1**. In the HMBC spectrum, the correlations from H-7a (δ_H 1.81) to C-3 (δ_C 195.2), C-4 (δ_C 62.0), and C-5 (δ_C 208.0), and from H_2-17 (δ_H 2.62) and H_2-22 (δ_H 2.77) to C-1 (δ_C 194.2), C-5 (δ_C 208.0), and C-6 (δ_C 61.0), together with the chemical shifts of two carbonyls (δ_C 195.2 and 208.0) in the phloroglucinol core indicated that the two carbonyl groups were located at C-3 and C-5 in **2**, respectively, different at C-1 and C-5 (δ_C 193.3 and 213.9) in **1** [23,24]. Moreover, detailed inspection of their ^{13}C NMR data showed that the chemical shifts of C-13 in **2** (δ_C 85.4) were obviously shifted downfield than that in **1** (δ_C 68.8). Therefore, the hydroperoxyl group was deduced to be attached at C-13 in **2**, which could be further proved by the HMBC correlations of H-12 (δ_H 1.69), H_2-14 (δ_H 2.10), and Me-15 (δ_H 1.24) with C-13 (δ_C 85.4) [19]. The cross-peaks of H-29/H-14b and H-29/H-7b shown in its ROESY spectrum demonstrated that the benzoyl group was on the underside of the cyclohexane moiety. So, the structure of **2** was elucidated as exhibited.

Hyperpatulol C (**3**) shared the identical molecular formula of $C_{26}H_{38}O_6$ as chipericumin C [23] based on its HRESIMS spectrum and ^{13}C NMR data. The differences in C-15 (δ_C 23.9 in **3**; 21.1 in chipericumin C) and C-17 (δ_C 21.7 in **3**; 26.2 in chipericumin C) between **3** and chipericumin C implied that they were stereoisomeric at C-6 and C-13. The ROE correlations of H-14b/Me-15, Me-15/H-12, Me-17/H-14b and H-19/H-7b indicated that Me-15 and Me-17 were α-oriented. Therefore, the structure of **3** was constructed as shown.

The molecular formula of hyperpatulol D (**4**) was deduced to be same as that of **3** by its ^{13}C NMR and HRESIMS spectra. Comparison of their 1D and 2D NMR data showed that the planar structures of **3** and **4** were identical. The relative configurations of **4** were assigned based on the ROESY analysis and by comparison of their ^{13}C NMR data. Compared to those of **3**, the signals of C-7 (δ_C 29.8 in **4**; 32.3 in **3**), C-8 (δ_C 44.7 in **4**; 47.9 in **3**) and C-13 (δ_C 70.6 in **4**; 72.5 in **3**) obviously shifted upfield, while the signals of C-14 (δ_C 44.6 in **4**; 42.0 in **3**) and C-15 (δ_C 29.1 in **4**; 23.9 in **3**) shifted downfield, suggesting the differences between **4** and **3** in the stereochemistry of C-4, C-8, C-12, and C-13. The ROE correlations of H-12/H-7a, H-12/H-14a, H-12/Me-15, Me-15/H-14a, H-12/Me-16, and H-7a/Me-16 indicated the β-orientation for H-7a, H-12, H-14a, Me-15 and Me-16 and the chair conformation of the cyclohexane moiety. The ROE interactions of H-8 with H-7b and H-14b revealed the α-orientation for H-8 and the trans-fused conformation of the cyclohexane and cyclopentane moieties. In addition, the ROE correlations of H-24/H-14b and H-24/H-7b showed that the methylpropanoyl group was on the underside of the cyclohexane moiety. So, the structure of **4** was established as displayed in Fig. 1.

Hyperpatulol E (**5**), a light yellow gum, possessed the molecular formula of $C_{27}H_{40}O_6$ elucidated by its ^{13}C NMR spectrum and the observed HRESIMS data (*m/z* 483.2715 $[M+Na]^+$). The structures of **4** and **5** were quite similar, apart from the substituent at C-2. The 2-methylpropanoyl group in **4** was replaced by a 2-methylbutanoyl group (δ_H 3.44, 1H, m; 1.75, 1H, m; 1.46, 1H, m; 1.17, 3H, d, J = 6.7 Hz; 0.89, 3H, t, J = 7.4 Hz; δ_C 207.6, 41.3, 27.7, 16.8, 11.9) in **5**. Thus, the structure of hyperpatulol E was concluded as **5** in Fig. 1.

The HRESIMS spectrum of **6** showed its molecular formula as $C_{26}H_{38}O_7$, 16 mass units more than **3**. Its spectroscopic data (Table 2) were closely similar to those of **3** and the main difference between them was at C-12. The signal of C-12 obviously shifted downfield from δ_C 51.6 in **3** to δ_C 81.5 in **6**. Considering 16 mass units more than **3**, a hydroxyl group might be located at C-12 [25] (Fig. 2). This conclusion was deduced by the HMBC cross-peaks from Me-15 (δ_H 1.37) to C-12 (δ_C 81.5), C-13 (δ_C 74.1), and C-14 (δ_C 33.8), and from H-14a (δ_H 2.33) to C-3 (δ_C 195.7), C-4 (δ_C 60.3), and C-5 (δ_C 214.1). Besides, the correlations of Me-15/H-8, Me-15/H-14a, H-8/H-14a, H-8/Me-16, and H-11a/Me-15 were observed in its ROESY spectrum, suggesting that Me-15 and H-11a was β-oriented. Thus, the structure of **6** was determined and named hyperpatulol F.

Hyperpatulols G (**7**) and H (**8**) possessed the identical molecular formula of $C_{27}H_{38}O_5$ with nine indices of hydrogen deficiency determined by their HRESIMS and ^{13}C NMR spectra. The resemblance in the 1D and 2D NMR data of **7** and **8** indicated that their planar structures were identical and quite similar to sampsonol E [24]. The only difference between **7** and sampsonol E was the side chain at C-2. The 2-methylpropanoyl group in sampsonol E was substituted by a 2-methylbutanoyl group (δ_H 3.01, 1H, m; 1.72, 1H, m; 1.34, 1H, m; 1.10, 3H, d, J = 6.9 Hz; 0.86, 3H, t, J = 7.6 Hz; δ_C 203.7, 46.7, 25.5, 15.4, 11.6) in **7** (Fig. 2). In addition, the chemical shift of C-12 upfield-shifted from δ_C 47.6 in **7** to δ_C 44.8 in **8**, suggesting that **7** and **8** might be C-12 epimers. The ROE interactions of H-12 with H-7a and Me-16 confirmed the β-orientation for H-12 in **8**. Thus, the structures of **7** and **8** were

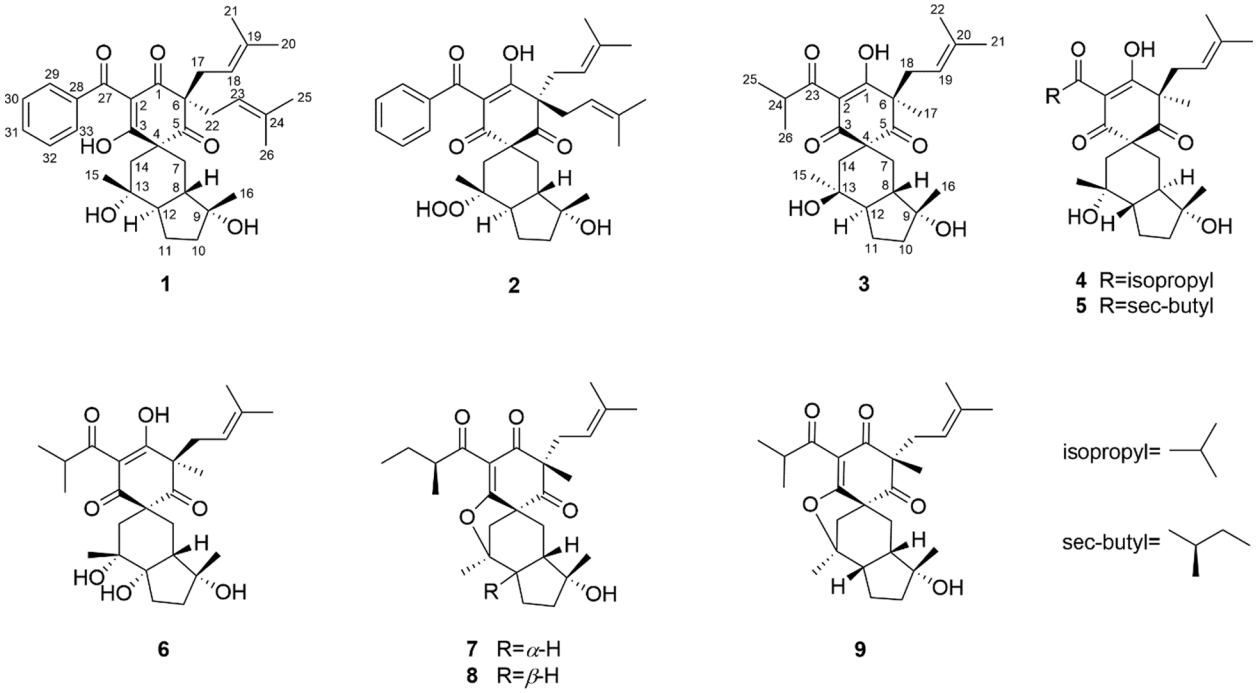

Fig. 1. Structures of compounds **1–9.**

elucidated as shown.

The HRESIMS spectrum of hyperpatulol I (**9**) gave a molecular formula of $C_{26}H_{36}O_5$, 14 mass units less than that of **7** and **8**. Its planar structure was established to be same as that of sampsonol F [24] based on its 1D and 2D NMR data. The difference in C-12 (δ_C 44.8 in **9**; 47.6 in sampsonol F) between **9** and sampsonol F implied that they were C-12 epimers. Detailed ROESY analysis revealed that the stereochemistry of **9** at C-4, C-6, C-8, C-9, C-12, and C-13 was same as those of **8**, determined by the ROE correlations of H-8/Me-16, H-12/Me-16, H-12/H-7a, H-7b/Me-15, H-24/H-7a, and Me-17/H-7b and by comparing their ^{13}C NMR data. Therefore, compound **9** was illustrated as shown.

The absolute configurations of compounds **1–9** were determined by the electronic circular dichroism (ECD) exciton chirality method and further confirmed by time-dependent density functional theory (TDDFT) ECD calculation. The observed positive chirality in the ECD spectra of **1**, **3** and **6–9** resulting from the coupling of two excitons (the n–π* transition of β-oxygenated conjugated enone group and the n–π* transition of nonconjugated carbonyl bond) indicated that two chromophores were arranged in the clockwise manner in space (Fig. 3A) [26,27]. Therefore, their absolute configurations were assigned as depicted. Meanwhile, the absolute configurations of **2**, **4** and **5** were defined by the negative chirality resulting from the same exciton coupling

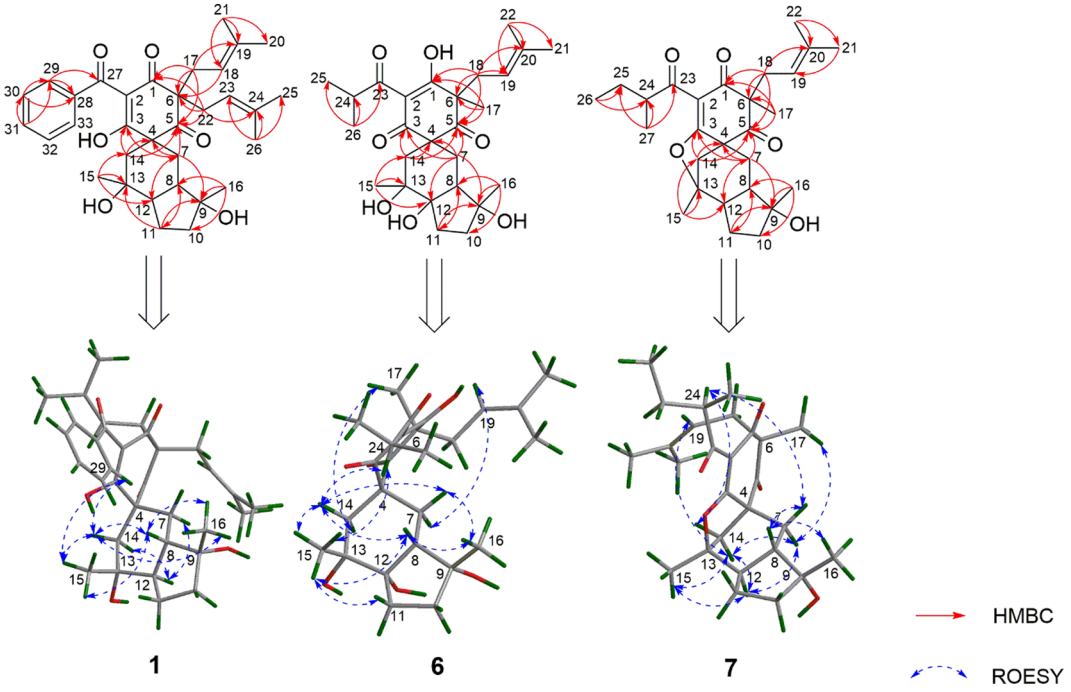

Fig. 2. Key HMBC and ROESY correlations of **1**, **6** and **7**.

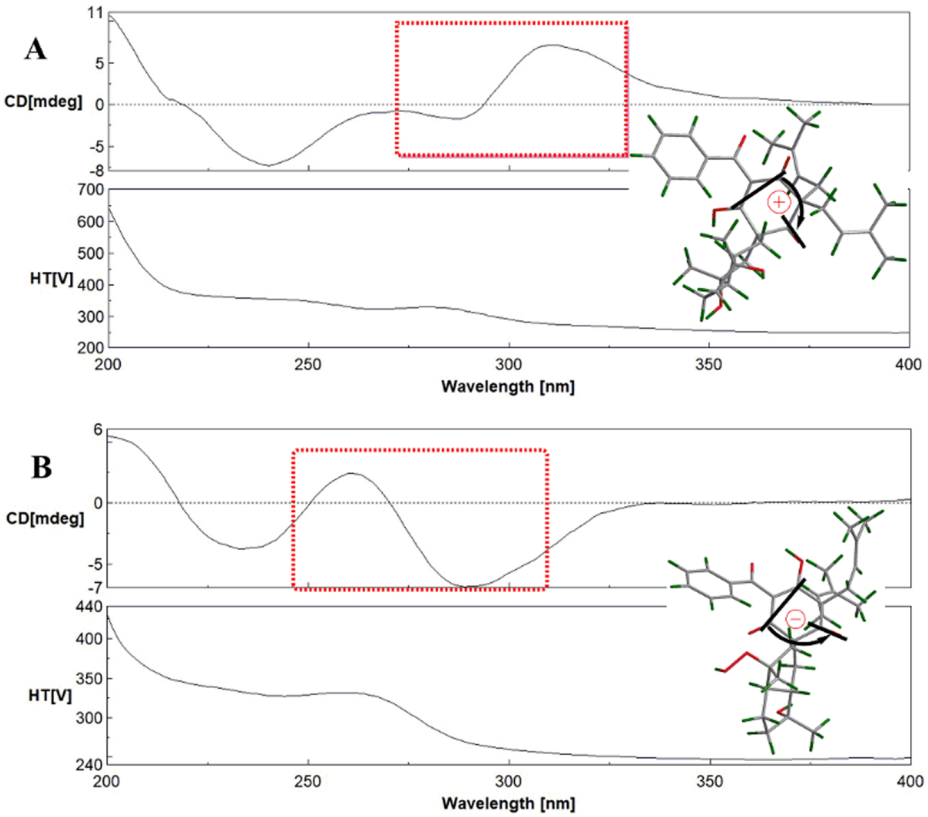

Fig. 3. ECD and UV spectra of **1** (A) and **2** (B). The bold lines denote the electric transition dipoles of the chromophores.

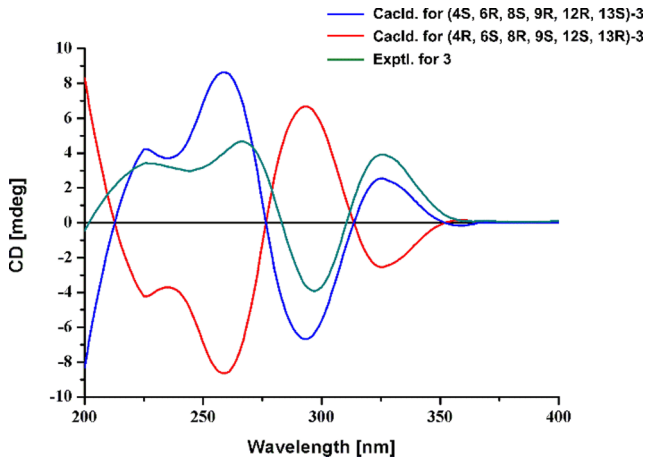

Fig. 4. Experimental and calculated ECD spectra of **3**.

showed in their ECD spectra, which revealed the counterclockwise space arrangement of two chromophores (Fig. 3B). In order to confirm the above conclusions, the absolute configuration of **3** was further evaluated by ECD calculation [2,28]. The calculated ECD spectrum of the conformer determined by the ECD exciton chirality method matched very well with the experimentally observed spectrum in MeOH (Fig. 4), which confirmed the absolute configuration determined by the ECD exciton chirality method. Thus, the structures of **1**–**9** were assigned as depicted. Moreover, the absolute configurations of C-24 in all reported PPAPs were *S* [29,30]. Biogenetically, compounds **5**, **7** and **8** were all derived from the precursor chinesin I, and the absolute configurations (24*S*) in **5**, **7** and **8** were retained during the formation [6,29]. Therefore, from the view of biogenetics, the absolute configurations of C-24 in **5**, **7** and **8** were all assigned as 24*S*.

3.2. Anti-migration activity

Previous pharmacological investigations indicated that PPAPs showed potential inhibition activity against tumor cells migration [31]. In order to test their anti-migration activities, the cytotoxicity of compounds **1**–**9** was firstly screened with U2-OS human osteosarcoma cells by MTT assay. The results revealed that all isolates showed no cytotoxicity on the U2-OS human osteosarcoma cells (IC_{50} > 100 μM). Subsequently, the anti-migration activities of compounds **1**–**9** against U2-OS cells were further evaluated through wound healing assay. As shown in Fig. 5A, compound **2** exhibited the stronger inhibitory activity than **1**, suggesting that the peroxyhydroxy group at C-13 might enhanced the anti-migration activities of spirocyclic acylphloroglucinol derivatives. For compounds **4** and **5**, **4** showed the stronger activity, demonstrating that the configuration of C-8 and the substituent at C-2 might play a vital role in the observed activity. Considering the potential anti-migration activity exhibited by compound **4**, its anti-migration activity was further studied by wound healing assay and transwell assay. As shown in Fig. 5B and C, compound **4** could suppress the migration of U2-OS cells in a dose-dependent manner. All the above results indicated that spirocyclic acylphloroglucinol derivatives possessed potential anti-migration activity.

Epithelial-mesenchymal transition (EMT) has emerged as an important determinant role in cancer metastasis [32]. As the common markers, the up-regulation of Vimentin and down-regulation of E-cadherin are the key steps in the EMT process [33,34]. In order to research on the mechanism of the anti-migration activity of compound **4**, further immunoblot analysis was carried out to reveal the influences of **4** on the expressions of E-cadherin and Vimentin with GAPDH as a control. The Western blotting results (Fig. 5D) indicated that compound **4** could down-regulate the expression of Vimentin, and up-regulate the expression of E-cadherin, indicating that **4** could suppress the EMT process and repress the migration of osteosarcoma cells [35,36]. Overall, **4**

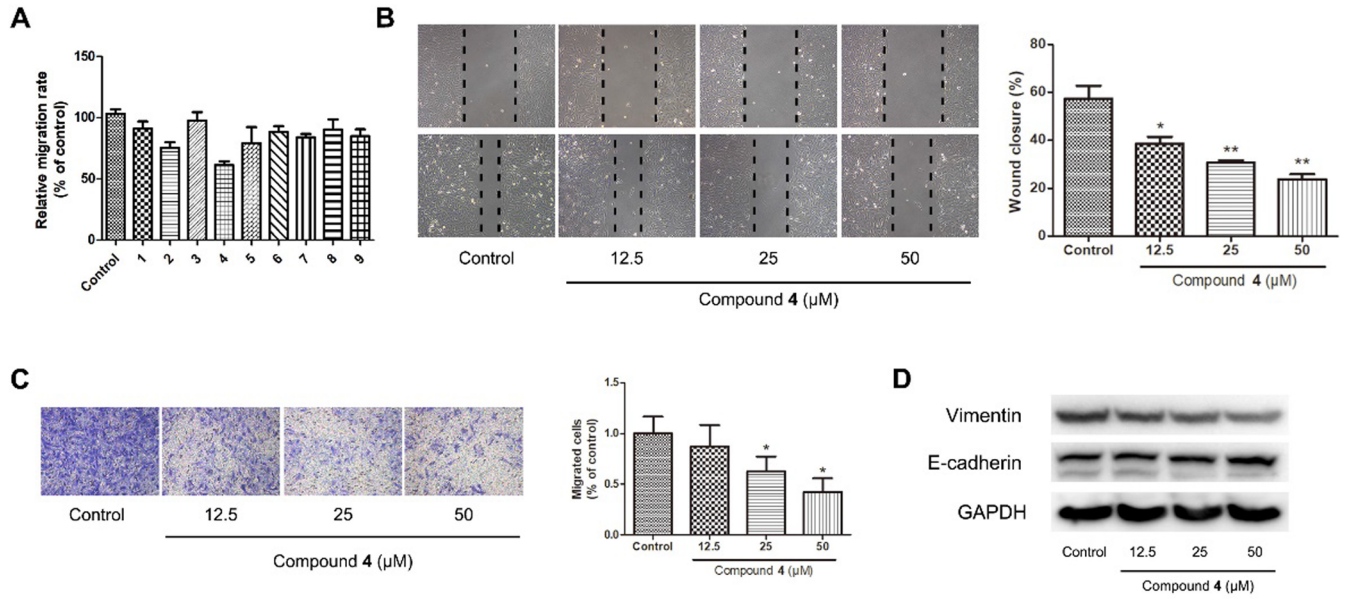

Fig. 5. Anti-migration activities of compounds **1–9** against U2-OS cells. (A) Effects of compounds **1–9** on U2-OS cells migration. (B) Wound healing assay on U2-OS cells with compound **4** in different concentrations (12.5, 25 and 50 μM). (C) Transwell assay on U2-OS cells with compound **4** in different concentrations (12.5, 25 and 50 μM). (D) Effects on the expression of Vimentin and E-cadherin with compound **4** in different concentrations (12.5, 25 and 50 μM) with GAPDH as a control.

could inhibit the migration of U2-OS cells by regulating the expressions of Vimentin and E-cadherin to suppress the EMT process. This is the first research on the mechanism of the anti-migration activity of PPAPs.

4. Conclusion

Phytochemical studies on the flowers of *H. patulum* revealed nine new spirocyclic acylphloroglucinol derivatives, hyperpatulols A–I (**1–9**). All the isolates were tested for their anti-migration activities against U2-OS human osteosarcoma cells. Among them, compound **4** showed moderate inhibitory activity against U2-OS cells in a dose-dependent manner, which was related to the regulation of the proteins E-cadherin and Vimentin.

Acknowledgments

This research work was supported by the National Natural Science Foundation of China (81773886), the 111 Project from Ministry of Education of China and the State Administration of Foreign Export Affairs of China (B18056), and High Performance Computing Center, China Pharmaceutical University.

Conflict of interest

The authors declare no competing financial interest.

Appendix A. Supplementary material

Supplementary data to this article can be found online at https://doi.org/10.1016/j.bioorg.2019.03.025.

References

[1] E. Napoli, L. Siracusa, G. Ruberto, A. Carrubba, S. Lazzara, A. Speciale, F. Cimino, A. Saija, M. Cristani, Phytochemistry 152 (2018) 162–173, https://doi.org/10.1016/j. phytochem.2018.05.003.
[2] W.J. Xu, R.J. Li, O. Quasie, M.H. Yang, L.Y. Kong, J. Luo, J. Nat. Prod. 79 (2016) 1971–1981, https://doi.org/10.1021/acs.jnatprod.6b00251.
[3] S. Dresler, J. Kováčik, M. Strzemski, I. Sowa, M. Wójciak-Kosior, J. Pharm. Biomed. Anal. 155 (2018) 82–90, https://doi.org/10.1016/j.jpba.2018.03.048.
[4] P.T. Nedialkov, Y. Ilieva, G. Momekov, Z. Kokanova-Nedialkova, Fitoterapia 127 (2018) 375–382, https://doi.org/10.1016/j.fitote.2018.03.011.
[5] Y. Guo, N. Zhang, C. Chen, J. Huang, X.N. Li, J. Liu, H. Zhu, Q. Tong, J. Zhang, Z. Luo, Y. Xue, Y. Zhang, J. Nat. Prod. 80 (2017) 1493–1504, https://doi.org/10.1021/acs.jnatprod. 6b01178.
[6] X.W. Yang, R.B. Grossman, G. Xu, Chem. Rev. 118 (2018) 3508–3558, https://doi.org/10.1021/acs.chemrev.7b00551.
[7] S. Chaturonrutsamee, C. Kuhakarn, P. Surawatanawong, S. Prabpai, P. Kongsaeree, T. Jaipetch, P. Piychaturawat, S. Jariyawat, R. Akkarawongsapat, K. Suksen, J. Limthongkul, C. Napaswad, N. Nuntasaen, V. Reutrakul, Phytochemistry 146 (2018) 63, https://doi.org/10.1016/j.phytochem.2017.12.001.
[8] X.W. Yang, Y.P. Li, J. Su, W.G. Ma, G. Xu, Org. Lett. 18 (2016) 1876–1879, https://doi.org/10.1021/acs.orglett.6b00650.
[9] Y.P. Li, K. Hu, X.W. Yang, G. Xu, J. Nat. Prod. 81 (2018) 1098–1102, https://doi.org/10.1021/acs.jnatprod.8b00017.
[10] S.X. Huang, C. Feng, Y. Zhou, G. Xu, Q.B. Han, C.F. Qiao, D.C. Chang, K.Q. Luo, H.X. Xu, J. Nat. Prod. 72 (2009) 130–135, https://doi.org/10.1021/np800496c.
[11] H. Zhu, C. Chen, J. Liu, B. Sun, G. Wei, Y. Li, J. Zhang, G. Yao, Z. Luo, Y. Xue, Y. Zhang, Phytochemistry 115 (2015) 222–230, https://doi.org/10.1016/j.phytochem.2015.02.009.
[12] B. Martinez-Poveda, A.R. Quesada, M.A. Medina, Int. J. Cancer. 117 (2005) 775–780, https://doi.org/10.1002/ijc.21246.
[13] W. Katja, M. Hans, H. Volker, H. David, W. Oliver, J. Johann, Eur. J. Med. Chem. 101 (2015) 133–149, https://doi.org/10.1016/j.ejmech.2015.06.001.
[14] Y. Shimizu, S.L. Shi, H. Usuda, M. Kanai, M. Shibasaki, Angew. Chem. Int. Ed. 49 (2010) 1103–1106, https://doi.org/10.1002/anie.200906678.
[15] N. Biber, K. Möws, B. Plietker, Nat. Chem. 3 (2011) 938–942, https://doi.org/10.1038/nchem.1170.
[16] Chang Su New Medical College, Dictionary of Chinese Crude Drugs, Shanghai Scientific Technological Publishers, Shanghai, 1994, p. 1387.
[17] N. Tanaka, Y. Yano, Y. Tatano, Y. Kashiwada, Org. Lett. 18 (2016) 5360–5363, https://doi.org/10.1021/acs.orglett.6b02725.
[18] Y.Y. Liu, Z. Ao, G.M. Xue, X.B. Wang, J.G. Luo, L.Y. Kong, Org. Lett. 20 (2018) 7953–7956, https://doi.org/10.1021/acs.orglett.8b03523.
[19] X.Q. Chen, Y. Li, K.Z. Li, L.Y. Peng, J. He, K. Wang, Z.H. Pan, X. Cheng, M.M. Li, Q.S. Zhao, G. Xu, Chem. Pharm. Bull. 59 (2011) 1250–1253, https://doi.org/10.1248/cpb.59. 1250.
[20] E.L. Ghisalberti, Phytochemistry 41 (1996) 7–22, https://doi.org/10.1016/0031-9422(95) 00484-X.
[21] L. Carneiro Albernaz, A. Deville, L. Dubost, J.E. de Paula, B. Bodo, P. Grellier, L. Salmen Espindola, L. Mambu, Planta Med. 78 (2012) 459–464, https://doi.org/10.1055/s-0031-1298156.
[22] L.T. Nguyen, H.T. Nguyen, M. Barbič, G. Brunner, J. Heilmann, H.D. Pham, D.M. Nguyen, L.D. Nguyen, Tetrahedron Lett. 53 (2012) 4487–4493, https://doi.org/10.1016/j.tetlet.2012.05.096.
[23] S. Abe, N. Tanaka, J.I. Kobayashi, J. Nat. Prod. 75 (2012) 484–488, https://doi.org/10.1016/10.1021/np200741x.
[24] W.B. Xin, X.H. Man, C.J. Zheng, M. Jia, Y.P. Jiang, X.X. Zhao, G.L. Jin, Z.J. Mao, H.Q. Huang, L.P. Qin, Fitoterapia 83 (2012) 1540–1547, https://doi.org/10.1016/j.fitote. 2012.08. 022.
[25] H.M.R. Hoffmann, I. Miinnich, O. Nowitzki, H. Stucke, D.J. Williams, Tetrahedron 52 (1996) 11783–11798, https://doi.org/10.1016/0040-4020(96)00687-4.
[26] N. Berova, L. Di Bari, G. Pescitelli, Chem. Soc. Rev. 36 (2007) 914–931, https://doi.

org/10.1039/B515476F.
[27] K. Niwa, N. Tanaka, S.Y. Kim, M. Kojoma, Y. Kashiwada, Org. Lett. 20 (2018) 5977–5980, https://doi.org/10.1021/acs.orglett.8b02739.
[28] J.J. Zhang, J. Yang, Y. Liao, X.W. Yang, Q.L. Xiao, L.X. Yang, G. Xu, Org. Lett. 16 (2014) 4912–4915, https://doi.org/10.1021/ol502425f.
[29] W.J. Xu, J. Luo, R.J. Li, M.H. Yang, L.Y. Kong, Org. Chem. Front. 4 (2017) 313–317, https://doi.org/10.1039/c6qo00620e.
[30] W.J. Xu, M.D. Zhu, X.B. Wang, M.H. Yang, J. Luo, L.Y. Kong, J. Nat. Prod. 78 (2015) 1093–1100, https://doi.org/10.1021/acs.jnatprod.5b00066.
[31] L. Wang, R. Wu, W. Fu, Y. Lao, C. Zheng, H. Tan, H. Xu, Bioorg. Med. Chem. 24 (2016) 4120–4128, https://doi.org/10.1016/j.bmc.2016.06.054.
[32] E.L. Busch, K.A. McGraw, R.S. Sandler, Cancer Epidemiol. Biomarkers Prev. 23 (2014) 1164–1175, https://doi.org/10.1158/1055-9965.EPI-14-0017.
[33] B. De Craene, G. Berx, Nat. Rev. Cancer 13 (2013) 97–110, https://doi.org/10.1038/nrc 3447.
[34] X. Ye, R.A. Weinberg, Trends Cell Biol. 15 (2015) 675–686, https://doi.org/10.1016/j.tcb. 2015.07.012.
[35] X. Lin, L. Zheng, H. Song, J. Xiao, B. Pan, H. Chen, X. Jin, H. Yu, Exp. Mol. Pathol. 102 (2017) 522–532, https://doi.org/10.1016/j.yexmp.2017.05.009.
[36] J. Kong, W. Sun, C. Li, L. Wan, S. Wang, Y. Wu, E. Xu, H. Zhang, M. Lai, Cancer Lett. 380 (2016) 476–484, https://doi.org/10.1016/j.canlet.2016.07.015.